Spiral spin structures and origin of the magnetoelectric coupling in YMn_2O_5

J.-H. Kim,[1] S.-H. Lee,[1,*] S. I. Park,[2] M. Kenzelmann,[3] A. B. Harris,[4] J. Schefer,[3] J.-H. Chung,[5] C. F. Majkrzak,[6] M. Takeda,[7] S. Wakimoto,[7] S. Y. Park,[8] S-W. Cheong,[8] M. Matsuda,[7] H. Kimura,[9] Y. Noda,[9] and K. Kakurai[7]

[1]*Department of Physics, University of Virginia, Charlottesville, Virginia 22904-4714, USA*

[2]*Neutron Science Division, Korea Atomic Energy Research Institute, Daejeon 305-303, Korea*

[3]*Laboratory for Neutron Scattering, ETH Zurich and Paul Scherrer Institute, CH-5232 Villigen PSI, Switzerland*

[4]*Department of Physics and Astronomy, University of Pennsylvania, Philadelphia, Pennsylvania 19104, USA*

[5]*Department of Physics, Korea University, Seoul 136-713, Korea*

[6]*NIST Center for Neutron Research, National Institute of Standards and Technology, Gaithersburg, Maryland 20899, USA*

[7]*Quantum Beam Science Directorate, Japan Atomic Energy Agency, Tokai, Ibaraki 319-1195, Japan*

[8]*Department of Physics and Astronomy and Rutgers Center for Emergent Materials, Rutgers University, Piscataway, New Jersey 08854, USA*

[9]*Institute of Multidisciplinary Research for Advanced Materials, Tohoku University, Sendai 980-8577, Japan*

(Received 25 March 2008; revised manuscript received 26 September 2008; published 19 December 2008)

By combining neutron four-circle diffraction and polarized neutron-diffraction techniques we have determined the complex spin structures of a multiferroic YMn_2O_5 that exhibits two ferroelectric phases at low temperatures. The obtained magnetic structure has spiral components in both the low-temperature ferroelectric phases that are magnetically commensurate and incommensurate, respectively. Among proposed microscopic theories for the magnetoelectric coupling, our results are consistent with both the spin-current mechanism and the magnetostriction mechanism. Our results also explain why the electric polarization changes at the low-temperature commensurate-to-incommensurate phase transition.

DOI: 10.1103/PhysRevB.78.245115 PACS number(s): 75.25.+z

I. INTRODUCTION

Magnetic multiferroic materials become simultaneously ferroelectric and magnetic at low temperatures and are, thus, attractive for use in technological devices that can exploit both sets of properties.[1–5] It would, of course, be desirable to develop materials with such behavior at room temperature. To realize this goal it is necessary to obtain a full understanding of the origin of this behavior. For this purpose it is necessary to develop a precise determination of the magnetic and electronic structures of these materials. This program is complicated by the fact that typically such systems, as, for example, the AMn_2O_5 compounds where A is a rare earth, undergo several magnetic and electronic phase transitions upon cooling. To help clarify the situation we present here a detailed study of the magnetic structure of one member of this class of compounds, YMn_2O_5, in two of its magnetoelectric phases.

A. Overview of properties of AMn_2O_5

By way of introduction we first give a brief overview of the magnetoelectric properties of the AMn_2O_5. As long as one does not consider too low a temperature these systems display two scenarios of ordering.[6] At temperature above about $T_c=45$ K all these systems are in a high-temperature-paramagnetic-paraelectric (HTPM-PE) phase. Then at T_c the systems order into a state which is paraelectric but with magnetic order whose modulation vector has incommensurate x and z components so that this vector is nearly equal to the commensurate value $\mathbf{k_C}=(1/2,0,1/4)$ in reciprocal lattice units (rlu's). Then, a few degrees lower in temperature some of the AMn_2O_5 systems, $A=$Tb,[2,7–9] Ho,[10,11] and Dy (Refs. 12–15) follow the first scenario in which they make a phase transition into a phase [intermediate-temperature commensurate ferroelectric (ITC-FE)] which is ferroelectric and the magnetic order is commensurate with wave vector $\mathbf{k_C}$. In contrast, the AMn_2O_5 systems with $A=$Er,[16,17] Y,[18,19] and Tm (Ref. 20) follow the second scenario in which there is an intermediate phase between the paraelectric incommensurate magnetic phase and the commensurate ferroelectric phase ITC-FE. In this intermediate [intermediate-temperature incommensurate ferroelectric (ITI-FE)] phase only the x component of the magnetic wave vector is incommensurate and the state is ferroelectric. In either scenario the commensurate ferroelectric (ITC-FE) phase sets in at $T\approx 38$ K and persists down to temperatures of 5–25 K depending on the specific compound. At an even lower temperature, the ITC-FE state is replaced by a low-temperature [low-temperature incommensurate ferroelectric (LTI-FE)] state which is either incommensurate or a long period commensurate phase.[8,10,16,18,20] In this so-called ferroelectric phase the spontaneous polarization is either smaller [as in YMn_2O_5 (Ref. 21)] or possibly zero [as in $HoMn_2O_5$ (Ref. 10) or $ErMn_2O_5$ (Ref. 10)]. The experimental situation is reviewed in Ref. 6.

Up to now, the spontaneous polarization has only been observed along the **b** direction for $TmMn_2O_5$,[22] $DyMn_2O_5$,[12,13,23] $HoMn_2O_5$,[10,12,13,23] $ErMn_2O_5$,[10,17] $TbMn_2O_5$,[2,9,12,21,23] YMn_2O_5,[21,24] and $GdMn_2O_5$.[21] The emergence of a spontaneous polarization can also be inferred from an anomaly in the dielectric constant when measured along the **b** direction for $TmMn_2O_5$,[20] $DyMn_2O_5$,[12,14,23,25,26] $HoMn_2O_5$,[10,12,23,26] $ErMn_2O_5$,[10,16,17] $TbMn_2O_5$,[2,7,9,12,23,26] and YMn_2O_5.[18,24,27] Until recently the magnetic structure was thought to be more or less collinear.[19]

B. Theoretical background

Various theories have been proposed to explain the magnetoelectric coupling in magnetic multiferroics. These are naturally classified as microscopic or phenomenological. The microscopic theories usually begin with a Hubbard model or invoke a strain derivative of anisotropic spin-spin interactions. The first explanation was a microscopic calculation of Katsura *et al.*[28] involving a spin-current interaction. The spin current attributed to a pair of spin $\mathbf{S}_i$ and $\mathbf{S}_j$ is proportional to $\mathbf{S}_i \times \mathbf{S}_j$, and the resulting polarization was shown to be given by

$$\mathbf{P} = \text{const} \times \mathbf{e}_{ij} \times (\mathbf{S}_i \times \mathbf{S}_j), \tag{1}$$

where $\mathbf{e}_{ij}=(\mathbf{r}_i-\mathbf{r}_j)/|(\mathbf{r}_i-\mathbf{r}_j)|$, where $\mathbf{r}_i$ is the position of the ith spin and $\mathbf{e}_{ij}$ is a unit vector connecting the two magnetic ions. This mechanism requires the spins to be noncollinear. It should be mentioned that the spin-current model does not provide a universal explanation for magnetoelectricity, as is shown by the example of $RbFe(MoO_4)_2$, where the spins adopt a noncollinear structure but their orientations are confined to the hexagonal basal plane. According to Eq. (1) the polarization perpendicular to the basal plane should be zero.[29] But experiment clearly shows it to be nonzero.[30] This difficulty seems to be resolved by a recent analysis[31] of the symmetry of the microscopic interactions, which indicates the presence in Eq. (1) of a term proportional to $\mathbf{S}_i \times \mathbf{S}_j$, which would be consistent with the result for $RbFe(MoO_4)_2$.

An alternative calculation was given by Sergienko and Dagotto[32] who used the fact that even if the Dzialoshinskii-Moriya (DM) interaction vanished in an inversion symmetric structure, the DM interaction could lead to the kind of spin-phonon coupling that would lead to ferroelectricity. A more general analysis for the specific system $Ni_3V_2O_8$ was also given by Harris *et al.*[33] There it was shown that gradients of *any* of the components of the exchange tensor could lead to ferroelectricity provided the magnetic structure was such as to break inversion symmetry. Thus, if the spin structure has been fixed and proven to be of suitable character, it is not necessary any more to invoke the DM interaction. Reference 34 presents a theory based on magnetostriction in which $\mathbf{P} \propto \mathbf{S}_i \cdot \mathbf{S}_j$ can occur for a collinear spin structure that has $\uparrow\uparrow\downarrow\uparrow$ configuration in the antiferromagnetic nearest-neighbor spin interaction system. This spin structure leads to frustration. To release frustration, ions with parallel spins move away from each other, while ions with antiparallel spins move closer to each other. The displacements of these frustrated ions result in an electric polarization. Note that this theory is a special case of that of Ref. 33 in which all components of the exchange tensor are allowed to have a strain dependence. Their model, as well as the Landau model (see below), explains the magnetoelectric phenomena found in many different materials such as $TbMnO_3$ (Refs. 1, 35, and 36) and $CoCr_2O_4$.[37]

In principle, the phenomenological theories apply independently of the details of the microscopic mechanisms responsible for ferroelectricity. The advantage of such theories is that they enable one to incorporate the symmetry of the unit cell, a property which is crucial to multiferroics. In the initial Landau theory[35,38] the magnetoelectric coupling responsible for ferroelectricty involved a trilinear interaction of the form

$$V = i \sum_{\gamma=x,y,z} r_\gamma [\sigma_1(\mathbf{q})\sigma_2(\mathbf{q})^* - \sigma_1(\mathbf{q})^*\sigma_2(\mathbf{q})]P_\gamma, \tag{2}$$

where r_γ is a real constant and $\sigma_n(\mathbf{q})$ is a complex-valued order parameter specifying the amplitude of the incommensurate spin structure. The two order parameters describe spin patterns of different symmetry, which usually are the longitudinal and transverse components of a spin spiral. Because the order parameters are constructed to reflect the symmetry properties of the magnetic structure, it is usually trivial to determine which of the r_γ's are allowed to be nonzero.[39] For the commensurate state of the AMn_2O_5 systems the interaction is slightly different,[39,40]

$$V = \sum_{\gamma=x,y,z} r_\gamma [|\sigma_1(\mathbf{q})|^2 - |\sigma_2(\mathbf{q})|^2]P_\gamma. \tag{3}$$

These theories (as do others) predict correctly the orientation of the spontaneous polarization (along the **b** axis) and rely only on the symmetry of the magnetic structure and, in particular, give the correct result whether the spin structure in the AMn_2O_5 is a spiral (as now believed) or is more or less collinear (as previously believed), as long as the symmetry of the magnetic structure is correctly identified (this is usually easy to do).

An alternative phenomenological theory was advanced by Mostovoy.[41] This theory may be described as a macroscopic version of the spin-current model in that the symmetries of the two models are identical. A big advantage of the continuum model of Mostovoy[41] is that it provides an easily visualized picture of a magnetic structure (a magnetic spiral) that leads to ferroelectricity.[34,41] However, it has the drawback of the spin-current model in that it does not give a universal explanation of ferroelectricity, and, perhaps more important, it is not a convenient starting point from which to incorporate symmetry of the unit cell.[29] Furthermore one can clearly see that results such as Eq. (2) or (3) allow for a quantitative prediction of the temperature dependence of the spontaneous polarization.

A somewhat different phenomenological approach was proposed by Betouras *et al.*,[42] who invoked a spin-polarization interaction, which, in the language of Eq. (2), involved umklapp terms in the magnetoelectric interaction. This suggestion was elaborated in Ref. 40 where it was shown that this umklapp magnetoelectric interaction, though expected to be small, could nevertheless lead to nonzero components of the polarization, which were otherwise predicted to vanish. In the original paper of Betouras *et al.*[42] it was pointed out that that mechanism implied a lattice distortion at twice the periodicity of the unit cell. However, this was evaluated for a magnetic structure which doubled the unit cell, whereas for the AMn_2O_5 the cell is quadrupled in one direction. Perhaps a more detailed analysis of this effect is desirable.

TABLE I. Positions (in units of the orthorhombic lattice constant) of Mn ions in two chemical unit cells.

Site	Mn^{3+}	Mn^{4+}
1	(0.088, 0.851, 0.5)	(0.5, 0, 0.255)
2	(0.912, 0.149, 0.5)	(0, 0.5, 0.255)
3	(0.412, 0.351, 0.5)	(0, 0.5, 0.745)
4	(0.588, 0.649, 0.5)	(0.5, 0, 0.745)
5	(0.088, 0.851, 1.5)	(0.5, 0, 1.255)
6	(0.912, 0.149, 1.5)	(0, 0.5, 1.255)
7	(0.412, 0.351, 1.5)	(0, 0.5, 1.745)
8	(0.588, 0.649, 1.5)	(0.5, 0, 1.745)

C. Crystal and magnetic structure of YMn_2O_5

YMn_2O_5 (orthorhombic space group *Pbam*) has a complex crystal structure.[43] There are eight Mn ions at two distinct sites in the chemical unit cell (see Table I): one is the octahedral site occupied by the Mn^{4+} ($3d^3$; $S=3/2$) ions and the other is the pyramid site occupied by the Mn^{3+} ($3d^4$; $S=2$) ions. The neighboring $Mn^{4+}O_6$ octahedra along the *c* axis share edges and form a chain. The $Mn^{4+}O_6$ octahedra share corners with neighboring $Mn^{3+}O_5$ trigonal bipyramids and form a zigzag chain in the *ab* plane. Previous powder neutron-diffraction studies on AMn_2O_5 ($A=$Y and Tb) by Chapon *et al.*[8,19] reported nearly collinear spin structures along a zigzag chain for their ferroelectric phases and, thus, presented these systems as examples where the magnetostriction mechanism rather than the spin-current model is operative. In the previous study, the decrease in **P** at the transition from the ITC-FE to the LTI-FE phase was attributed to a magnetic transition from a structure with magnetic moments of similar amplitudes to an amplitude-modulated sinusoidal spin structure. The same result was also invoked as experimental evidence for a recent theory based on umklapp interactions.[42]

This discussion raises two questions. First, to what extent can one distinguish between the various theoretical modes on the basis of the structure determinations we are about to undertake? Second, what is the best experimental approach to uniquely determine a complex spin structure? The group theoretical analysis (representation theory) is a basic method to describe a complicated magnetic structure. This theory explains that the possible magnetic structure is limited by symmetry of the crystal structure of the paramagnetic phase when it undergoes a continuous phase transition and close to the paramagnetic phase. Recently, Harris[39] proposed that representation analysis with considering inversion symmetry can decrease the number of parameters needed to construct the spin structure in ITC-FE of AMn_2O_5. According to this idea, determining the spin structure of YMn_2O_5 requires optimization of 14 parameters excluding an overall scale factor for ITC-FE phase. (The most convenient parametrization is given in Ref. 40.) However, this analysis is not applicable for the low-temperature incommensurate phase since this phase probably cannot be reached without crossing a first-order phase boundary. (Representation theory is not applicable to a state reached only via a first-order transition.) Thus, for the LTI-FE phase, no restriction from symmetry was assumed so that 48 magnetic structure parameters excluding an overall scale parameter had to be optimized. While powder diffraction is not sufficient to find a complex spin structure due to its intrinsic powder averaging, four-circle diffraction (FCD) from a single crystal can probe each wave vector separately and, thus, provide much more detailed information than powder diffraction. The FCD technique has been instrumental in studying many different magnetic multiferroics.[11,35,44] However, as we will see later, the FCD by itself is not enough when it comes to determining complex spin structures as in AMn_2O_5.

Here, we demonstrate that the combination of FCD and polarized neutron-diffraction (PND) techniques can lead to a unique determination of the complex spin structures of YMn_2O_5 and reveal the correct nature of the coupling of the magnetic and ferroelectric order parameters in both the ITC-FE and LTI-FE phases. Our spiral structure of the ITC-FE phase is consistent with recent FCD results.[44,45] We show that the LTI-FE phase also has a magnetic spiral structure that is much more complex than the ITC-FE phase and is different from the sinusoidal spin structure proposed by the previous powder neutron-diffraction study.[19] We give a detailed discussion and show that both the spin-current and the magnetostriction model[34] can explain the experimental result of **P** in the ITC-FE and LTI-FE phases. Other theoretical implications of the different spin structures of YMn_2O_5 are also discussed.

II. EXPERIMENT

A 1 g single crystal of YMn_2O_5 was used for our neutron FCD and PND measurements. In the FCD measurements relative spin directions and magnitudes in a magnetic system give rise to relative intensities of magnetic Bragg reflections, while in the PND measurements they give rise to different intensities in the non-spin-flip (NSF) and the spin-flip (SF) channels at each reflection. Thus, in the FCD technique, enough information for the structure determination can only be obtained by measuring a large number of reflections. As the complexity of the structure increases, the required number of reflections grows. In the PND technique, on the other hand, information about particular spin directions and magnitudes can be achieved at each reflection. Thus, the two techniques can be complementary and powerful, when combined, in determining a complex spin structure. Our FCD measurements were performed at the four-circle diffractometer, TriCS, at the Paul Scherrer Institute to collect about 300 magnetic reflections in ITC-FE at 25 K and LTI-FE phase at 10 K. Our PND measurements were done at two neutron facilities using two different experimental configurations. At the NG1 reflectometer at the National Institute of Standards and Technology, the conventional PND measurements were performed with two sets of transmission neutron polarizers and spin flippers before and after the sample, and a vertical guide field along the beam path to maintain the selected spin state of neutrons. At the Japan Atomic Energy Agency, the three-dimensional polarization analysis (CRYO-

PAD) technique was used at the TAS-1 spectrometer. In both PND measurements, the crystal was aligned in the $(h0l)$ scattering plane. Thus, in the conventional PND measurements, the b components of the magnetic moments go to the non-spin-flip channel while the ac components go to the spin-flip channel. The polarization efficiency, i.e., the fraction of neutrons that are polarized along the selected directions, was measured at the nuclear reflections to be 82% for the conventional PND and 94% for the CRYOPAD measurements.

The three-dimensional polarization technique can measure different scattered-neutron polarization from the incident neutron polarization. The neutron-scattering cross section $\frac{d\sigma}{d\Omega}$ can be written as[46]

$$\frac{d\sigma}{d\Omega} = NN^* + N^*\vec{P}_i \cdot \vec{M}_\perp + N\vec{P}_i \cdot \vec{M}^*_\perp + \vec{M}_\perp \cdot \vec{M}^*_\perp + i\vec{P}_i \cdot (\vec{M}^*_\perp \times \vec{M}_\perp), \quad (4)$$

where N is the nuclear structure factor, $\vec{M}_\perp = \hat{Q} \times [\vec{M}(\vec{Q}) \times \hat{Q}]$ is the magnetic interaction vector, and $\vec{P}_i$ is the polarization vector of the incident neutrons. In the CRYOPAD experiment, we measure[46]

$$\vec{P}_f \frac{d\sigma}{d\Omega} = \vec{P}_i NN^* + \vec{M}_\perp N^* + \vec{M}^*_\perp N - i(\vec{P}_i \times \vec{M}_\perp N^* - \vec{P}_i \times \vec{M}^*_\perp N) + \vec{M}_\perp (\vec{P}_i \cdot \vec{M}^*_\perp) + \vec{M}^*_\perp (\vec{P}_i \cdot \vec{M}_\perp) - \vec{P}_i (\vec{M}_\perp \cdot \vec{M}^*_\perp) - i(\vec{M}_\perp \cdot \vec{M}^*_\perp), \quad (5)$$

where $\vec{P}_f$ is the polarization vector of the scattered neutrons. The measurement yields a 3×3 polarization matrix (the P matrix) for each magnetic reflection. For the case where $N=0$ and where the magnetic structure is noncollinear as in YMn_2O_5, the P matrix becomes

$$\vec{P}_f = \begin{pmatrix} -1 & 0 & 0 \\ \frac{-i(M^*_{\perp y}M_{\perp z} - M^*_{\perp z}M_{\perp y})}{\vec{M}_\perp \cdot \vec{M}^*_\perp} & \frac{M_{\perp y}M^*_{\perp y} - M_{\perp z}M^*_{\perp z}}{\vec{M}_\perp \cdot \vec{M}^*_\perp} & \frac{M_{\perp z}M^*_{\perp y} + M^*_{\perp z}M_{\perp y}}{\vec{M}_\perp \cdot \vec{M}^*_\perp} \\ \frac{-i(M^*_{\perp y}M_{\perp z} - M^*_{\perp z}M_{\perp y})}{\vec{M}_\perp \cdot \vec{M}^*_\perp} & \frac{M_{\perp y}M^*_{\perp z} + M^*_{\perp y}M_{\perp z}}{\vec{M}_\perp \cdot \vec{M}^*_\perp} & \frac{M_{\perp z}M^*_{\perp z} - M_{\perp y}M^*_{\perp y}}{\vec{M}_\perp \cdot \vec{M}^*_\perp} \end{pmatrix} \vec{P}_i, \quad (6)$$

where x axis represents the direction parallel to the scattering vector $\vec{Q}$, y axis represents the horizontal axis perpendicular to $\vec{Q}$, and z axis the vertical direction with respect to the scattering plane. (See Ref. 46 for the detailed descriptions.) Now, due to the existence of crystal and magnetic domains, the off-diagonal terms vanish because our measurements were done without any external electric field. Thus, we used the two diagonal terms, $P_{yy} = -P_{zz}$ for our data analysis. P_{zz} corresponds to $\frac{I_{\mathrm{NSF}} - I_{\mathrm{SF}}}{I_{\mathrm{NSF}} + I_{\mathrm{SF}}}$ in terms of the conventional PND technique, where I_{NSF} and I_{SF} are the non-spin-flip and spin-flip neutron-scattering intensities, respectively. The experimental data from the CRYOPAD and conventional PND techniques were the same within the experimental error.

III. MAGNETIC STRUCTURES

Figure 1 shows our experimental data obtained from a single crystal of YMn_2O_5 at 25 K (ITC-FE phase) [Figs. 1(a) and 1(b)] and 10 K (LTI-FE phase) [Figs. 1(c) and 1(d)], along with model calculations based on several different spin structures. As shown as blue diamonds, the nearly collinear coplanar spin structures that were obtained by a previous neutron powder-diffraction study[19] cannot reproduce our FCD and PND data in both phases. Recently, for the commensurate ITC-FE phase, noncollinear spin structures were found based on FCD measurements, in which the ac and the bc components of Mn^{4+} ions form cycloidal spirals along the c axis.[44,45] As shown in Fig. 1(b), however, their spin structures do not perfectly reproduce our PND data (see cyan diamonds and purple crosses). This tells us that there may be several spin structures that can reproduce the FCD data, yet yield different polarized neutron data. Indeed, when we fit our FCD data for the ITC-FE phase, we could obtain several spin structures that are similar to but not the same as the previously reported noncollinear spiral spin structure, but which did not simultaneously fit our PND data. In order to obtain a spin structure that reproduces both the FCD and PND data well, we had to fit the FCD and PND data *simultaneously*. To our surprise, once the PND data were included in the fitting process, a direct least-squares refinement quickly converged after a few cycles to the spin structures that reproduced perfectly both FCD and PND data for the ITC-FE and LTI-FE phases. The results are shown by red stars in Fig. 1.

We fit the commensurate structure to the symmetry analysis of Ref. 39, but with the labeling of the sites given in Table IX of Ref. 40. We first consider the Mn^{3+} sites. Note that sites labeled 1, 2, 3, 4, 5, 6, 7, and 8 in that reference correspond to the labels 1, 4, 3, 2, 5, 6, 7, and 8 in the present

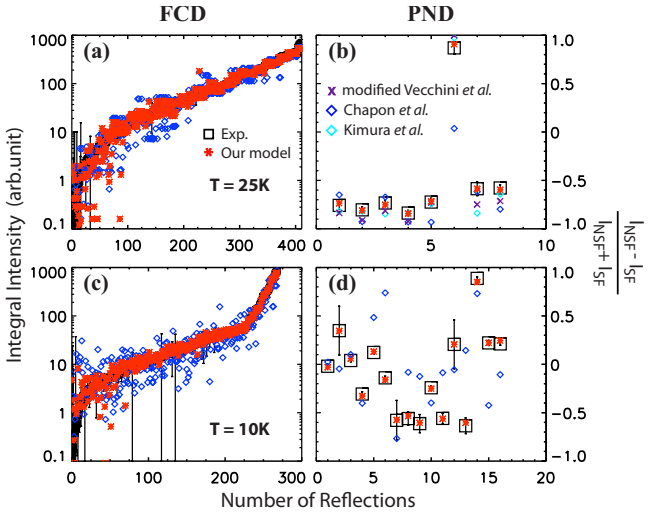

FIG. 1. (Color online) Four-circle diffraction (FCD) and polarized neutron diffraction (PND) data obtained from a single crystal of YMn_2O_5 [(a) and (b)] at 25 K (ITC-FE phase) and [(c) and (d)] at 10 K (LTI-FE). Red asterisks represent in (a) and (c) the calculated values for the unpolarized neutron FCD data at the magnetic Bragg reflections and in (b) and (d) those for the ratio of the PND data, $\frac{I_{NSF}-I_{SF}}{I_{NSF}-I_{SF}}$, that are obtained by our model as described in the text. Black squares represent the experimental data most of which are underneath the red asterisks in (a) and (c). Blue diamonds, cyan diamonds, and purple crosses represent the calculated values based on the magnetic structures reported by Chapon *et al.* (Ref. 19), by Kimura *et al.* (Ref. 45), and by modified Vecchini *et al.* (Ref. 44) (Table II), respectively. The experimental FCD data points shown in (a) and (c) were sorted by increasing intensity. The reflections of (b) are (2.5,0,−1.25), (0.5,0,−1.75), (1.5,0,−0.75), (0.5,0,−2.25), (0.5,0,−0.25), (1.5,0,−0.25), (1.5,0,−1.25), and (2.5,0,−1.75) in order. While the reflections of (d) are (2.52,0,−1.288), (0.48,0,−1.718), (1.48,0,−0.718), (0.52,0,−2.288), (0.52,0,−0.288), (1.52,0,−0.288), (1.52,0,−1.288), (2.48,0,−1.718), (2.48,0,−1.288), (0.52,0,−1.718), (1.52,0,−0.718), (0.48,0,−2.288), (0.48,0,−0.288), (1.48,0,−0.288), (1.48,0,−1.288), and (2.52,0,−1.718).

paper, in terms of which $M_\alpha(n)$, the α component of the magnetization at site n, is given by

$$M_\alpha(1) = \sigma_1 r_{1\alpha} + \sigma_2 r_{2\alpha} + \sigma_1^* r_{1\alpha}^* + \sigma_2^* r_{2\alpha}^*,$$

$$M_\alpha(2) = \sigma_1 \rho_\alpha r_{2\alpha} + \sigma_2 \rho_\alpha r_{1\alpha} + \sigma_1^* \rho_\alpha r_{2\alpha}^* + \sigma_2^* \rho_\alpha r_{1\alpha}^*,$$

$$M_\alpha(3) = \sigma_1 \tau_\alpha r_{1\alpha} - \sigma_2 \tau_\alpha r_{2\alpha} + \sigma_1^* \tau_\alpha r_{1\alpha}^* - \sigma_2^* \tau_\alpha r_{2\alpha}^*,$$

$$M_\alpha(4) = -\sigma_1 \xi_\alpha r_{2\alpha} + \sigma_2 \xi_\alpha r_{1\alpha} - \sigma_1^* \xi_\alpha r_{2\alpha}^* + \sigma_2^* \xi_\alpha r_{1\alpha}^*,$$

$$M_\alpha(5) = i\sigma_1 r_{1\alpha} + i\sigma_2 r_{2\alpha} - i\sigma_1^* r_{1\alpha}^* - i\sigma_2^* r_{2\alpha}^*,$$

$$M_\alpha(6) = i\sigma_1 \rho_\alpha r_{2\alpha} + i\sigma_2 \rho_\alpha r_{1\alpha} - i\sigma_1^* \rho_\alpha r_{2\alpha}^* - i\sigma_2^* \rho_\alpha r_{1\alpha}^*,$$

$$M_\alpha(7) = i\sigma_1 \tau_\alpha r_{1\alpha} - i\sigma_2 \tau_\alpha r_{2\alpha} - i\sigma_1^* \tau_\alpha r_{1\alpha}^* + i\sigma_2^* \tau_\alpha r_{2\alpha}^*,$$

$$M_\alpha(8) = -i\sigma_1 \xi_\alpha r_{2\alpha} + i\sigma_2 \xi_\alpha r_{1\alpha} + i\sigma_1^* \xi_\alpha r_{2\alpha}^* - i\sigma_2^* \xi_\alpha r_{1\alpha}^*, \quad (7)$$

where

$$\xi_x = -1, \quad \xi_y = 1, \quad \xi_z = -1,$$

$$\tau_x = 1, \quad \tau_y = -1, \quad \tau_z = -1,$$

$$\rho_x = -1, \quad \rho_y = -1, \quad \rho_z = 1. \quad (8)$$

Here the coefficients r_{1x}, r_{1y}, r_{2x}, and r_{2y} are all purely real constants, whereas r_{1z} and r_{2z} are pure imaginary constants. The σ's are complex-valued order parameters, which are the amplitudes of the two basis functions in the two-dimensional irreducible representation[39,47] appropriate to the wave vector in question.

For the Mn^{4+} sites we have

$$M_\alpha(1) = \sigma_1 \tau_\alpha z_\alpha^* + \xi_\alpha \sigma_2 z_\alpha^* + \sigma_1^* \tau_\alpha z_\alpha + \xi_\alpha \sigma_2^* z_\alpha,$$

$$M_\alpha(2) = \sigma_1 z_\alpha^* - \rho_\alpha \sigma_2 z_\alpha^* + \sigma_1^* z_\alpha - \rho_\alpha \sigma_2^* z_\alpha,$$

$$M_\alpha(3) = -\sigma_1 \rho_\alpha z_\alpha + \sigma_2 z_\alpha - \sigma_1^* \rho_\alpha z_\alpha^* + \sigma_2^* z_\alpha^*,$$

$$M_\alpha(4) = -\sigma_1 \xi_\alpha z_\alpha - \sigma_2 \tau_\alpha z_\alpha - \sigma_1^* \xi_\alpha z_\alpha^* - \sigma_2^* \tau_\alpha z_\alpha^*,$$

$$M_\alpha(5) = i\sigma_1 \tau_\alpha z_\alpha^* + i\xi_\alpha \sigma_2 z_\alpha^* - i\sigma_1^* \tau_\alpha z_\alpha - i\xi_\alpha \sigma_2^* z_\alpha,$$

$$M_\alpha(6) = i\sigma_1 z_\alpha^* - i\rho_\alpha \sigma_2 z_\alpha^* - i\sigma_1^* z_\alpha + i\rho_\alpha \sigma_2^* z_\alpha,$$

$$M_\alpha(7) = -i\sigma_1 \rho_\alpha z_\alpha + i\sigma_2 z_\alpha + i\sigma_1^* \rho_\alpha z_\alpha^* - i\sigma_2^* z_\alpha^*,$$

$$M_\alpha(8) = -i\sigma_1 \xi_\alpha z_\alpha - i\sigma_2 \tau_\alpha z_\alpha + i\sigma_1^* \xi_\alpha z_\alpha^* + i\sigma_2^* \tau_\alpha z_\alpha^*. \quad (9)$$

where the z's are complex quantities which have both real and imaginary parts.

TABLE II. The optimal values of the parameters in Eqs. (7) and (9) that yield our magnetic structure and the modified Vecchini *et al.*'s magnetic structure (Ref. 44) modified as described below Eq. (10).

	Our model	Modified Vecchini *et al.*'s model
σ_1	0	0
σ_2	5.07(6)+*i*7.70(4)	5.4(11)+*i*5.3(11)
$\mathbf{r}_1$	[−0.36(1), −0.10(1), *i*0.05(1)]	[−0.39(8), −0.10(2), *i*0.09(2)]
$\mathbf{r}_2$	[0.41(1), 0.10(1), *i*0.04(1)]	[0.42(8), 0.07(1), *i*0.06(1)]
$\mathbf{z}$	[0.28(1)+*i*0.03(1), −0.08(1)−*i*0.02(1), 0.03(1) −*i*0.05(1)]	[0.26(5)+*i*0.04(1), −0.06(1)−*i*0.01(1), 0.01(1) −*i*0.05(1)]

TABLE III. Magnetic moments of Mn^{3+} and Mn^{4+} ions in one quarter of the magnetic unit cell of the ITC-FE phase [$\mathbf{k_C}=(1/2,0,1/4)$] of YMn_2O_5, obtained by fitting the FCD and the PND data at 25 K. The positions are given as the coordinates of the magnetic ion in units of the chemical lattice constants, and M_a, M_b, M_c, and M are the a, b, and c components and the magnitude of the moments, respectively. The moments in next unit cells separated by (1,0,0) or (0,0,2) are opposite to the ones listed here, while those in the unit cell separated by (1,0,2) are the same as the listed ones. Errors for all parameters are given within parenthesis. The χ^2 was defined by $1/(N-N_p)\{\Sigma_{\mathrm{FCD}}[(I_{\mathrm{obs}}-I_{\mathrm{calc}})/\Delta I_{\mathrm{obs}}]^2+\Sigma_{\mathrm{PND}}[(P^{zz}_{\mathrm{obs}}-P^{zz}_{\mathrm{calc}})/\Delta P^{zz}_{\mathrm{obs}}]^2\}$ where $N=412$ which indicates the number of data points, the $N_p=15$ which is the number of the fitted parameters including an overall scale factor, and I_{obs} (ΔI_{obs}) is the FCD intensity (experimental error). $P^{zz}_{\mathrm{obs}}=(I_{\mathrm{NSF}}-I_{\mathrm{SF}})/(I_{\mathrm{NSF}}+I_{\mathrm{SF}})$ and $\Delta P^{zz}_{\mathrm{obs}}$ are the PND data and the experimental error. I_{calc} and P^{zz}_{calc} are the calculated values for I_{obs} and P^{zz}_{obs}, respectively. The optimal χ^2 was 61.4 for our model. The R factor that is defined by $\Sigma_{\mathrm{FCD}}(I_{\mathrm{obs}}-I_{\mathrm{cal}})/\Sigma_{\mathrm{FCD}}I_{\mathrm{obs}}\times 100(\%)$ was 9.74%. The modified Vecchini refers to our modification of their results to correspond to having only a single nonzero order parameter.

Our model

	Mn^{3+}				Mn^{4+}			
Site	M_a (μ_B)	M_b (μ_B)	M_c (μ_B)	M (μ_B)	M_a (μ_B)	M_b (μ_B)	M_c (μ_B)	M (μ_B)
1	2.08(4)	0.49(1)	−0.32(2)	2.16(4)	−1.68(4)	−0.58(2)	0.19(2)	1.79(5)
2	1.81(4)	0.52(1)	−0.35(1)	1.91(4)	1.68(4)	−0.58(2)	0.19(2)	1.79(5)
3	−2.08(4)	0.49(1)	−0.32(2)	2.16(4)	1.17(4)	−0.21(2)	0.51(2)	1.29(5)
4	1.81(4)	−0.52(1)	0.35(1)	1.91(4)	−1.17(4)	−0.21(2)	0.51(2)	1.29(5)
5	−3.16(3)	−0.74(1)	−0.21(2)	3.26(4)	2.00(4)	0.48(1)	0.47(2)	2.11(4)
6	−2.75(4)	−0.79(1)	−0.23(1)	2.87(4)	−2.00(4)	0.48(1)	0.47(2)	2.11(4)
7	3.16(3)	−0.74(1)	−0.21(2)	3.26(4)	−2.34(4)	0.72(1)	−0.01(1)	2.45(4)
8	−2.75(4)	0.79(1)	0.23(1)	2.87(4)	2.34(4)	0.72(1)	−0.01(1)	2.45(4)

Model of Vecchini *et al.* (Ref. 44)

	Taken from Ref. 44				Modified Vecchini				Taken from Ref. 44				Modified Vecchini			
Site	M_a	M_b	M_c	M	M_a	M_b	M_c	M	M_a	M_b	M_c	M	M_a	M_b	M_c	M
1	2.23(4)	0.42(6)	−0.33(8)	2.30(6)	2.26	0.39	−0.32	2.31	−1.71(6)	−0.44(7)	0.22(6)	1.78(8)	−1.63	−0.38	0.25	1.69
2	2.11(4)	0.46(6)	−0.42(9)	2.20(6)	2.12	0.52	−0.48	2.23	1.66(6)	−0.39(7)	0.20(7)	1.72(8)	1.63	−0.38	0.25	1.69
3	−2.25(4)	0.39(6)	−0.35(8)	2.31(4)	−2.26	0.39	−0.32	2.31	1.19(5)	−0.30(6)	0.37(9)	1.27(9)	1.18	−0.28	0.32	1.25
4	2.13(4)	−0.47(6)	0.40(9)	2.22(6)	2.12	−0.52	0.48	2.23	−1.11(5)	−0.28(5)	0.37(9)	1.20(9)	−1.18	−0.28	0.32	1.25
5	−2.23(4)	−0.42(6)	−0.33(8)	2.30(6)	2.21	−0.38	−0.32	2.27	1.16(5)	0.30(4)	0.33(8)	1.25(8)	1.15	0.28	0.32	1.22
6	−2.11(4)	−0.46(6)	−0.42(9)	2.20(6)	−2.08	−0.51	−0.49	2.19	−1.13(5)	0.26(4)	0.30(9)	1.20(8)	−1.15	0.28	0.32	1.22
7	2.25(4)	−0.39(6)	−0.35(8)	2.31(6)	2.21	−0.38	−0.32	2.27	−1.77(6)	0.44(7)	0.25(6)	1.84(8)	−1.61	0.38	0.25	1.67
8	−2.13(4)	0.47(6)	0.40(9)	2.22(6)	−2.08	0.51	0.49	2.19	1.65(6)	0.42(6)	0.25(6)	1.73(6)	1.61	0.38	0.25	1.67

The best fit was obtained with the parameters listed in Table II. The resulting values of the magnetic moments of Mn^{3+} and Mn^{4+} ions in one quarter of the magnetic unit cell for the ITC-FE phase are given in Table III and are illustrated in Fig. 2. Note that our optimal magnetic structure has only a single order parameter ($\sigma_1=0$, $\sigma_2\neq 0$) so expected by the Landau theory.[48] Furthermore, in Ref. 48 it was shown that the early results of Ref. 19 corresponded to $\sigma_1=0$ with $\mathbf{r}_1$ and $\mathbf{r}_2$ that are two dimensional in the ab plane, and the later results of Ref. 45 corresponded to $\sigma_2=0$ with three-dimensional $\mathbf{r}_1$ and $\mathbf{r}_2$. These two structures are clearly equivalent when only the ab components of the moments are considered, as higher terms in the Landau free energy can pick out a direction in σ space (e.g., $\sigma_1\sigma_2=0$, rather than $|\sigma_1|=|\sigma_2|$), but it should not break the equivalence between the two order parameters. In comparison, the results of Vecchini *et al.*[44] cannot be obtained by Eqs. (7) and (9). This is because our model has more strict restrictions on the magnetic structure due to the inversion symmetry resulting in the 14 parameters (without an overall parameter) than their model that has 26 parameters. Within our Landau theory, we could obtain a magnetic structure that is close to their model with two nonzero order parameters, using

$$\sigma_1 = 0.01 - i0.01, \quad \sigma_2 = 5.44 + i5.45,$$

$$\mathbf{r}_1 = (-0.39, -0.09, i0.08), \quad \mathbf{r}_2 = (0.41, 0.07, i0.06),$$

$$\mathbf{z} = (0.26 + i0.05, -0.06 - i0.01, 0.01 - i0.05). \quad (10)$$

One can see that $|\sigma_2| \gg |\sigma_1|$. When we require $\sigma_1=0$ but still try to find a magnetic structure that is close to the model of Vecchini *et al.*[44] and fits our data reasonably well [see Fig. 1(b)], we obtained a magnetic structure (we call it a modified Vecchini) with the parameters listed in Table II. This little exercise is to show that all reported magnetic structures for

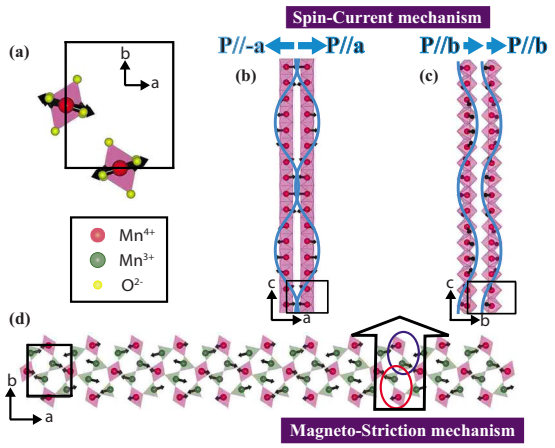

FIG. 2. (Color online) Magnetic structure of the ITC-FE phase of YMn_2O_5 that is projected onto different planes: (a) *ab* plane, (b) *ac* plane, and (c) *bc* plane. In (a)–(c), only Mn^{4+} (red spheres) and surrounding atoms of oxygen (yellow spheres) are shown. In (d), Mn^{4+} and Mn^{3+} (green spheres) ions are shown in the *ab*-plane projection. The thin black rectangle in each figure represents a chemical unit cell. Blue curves represent spirals formed by the magnetic ions. Thick blue arrows represent electric polarizations induced by the spirals according to the spin-current mechanism. The length of the arrow is scaled to the magnitude of **P**. The red and blue ellipses in (d) show Mn^{4+}-Mn^{3+}-Mn^{3+}-Mn^{4+} ions along the *b* axis with ↑↑↓↑ configuration which induces **P** along *b* axis by magnetostriction mechanism (Ref. 34).

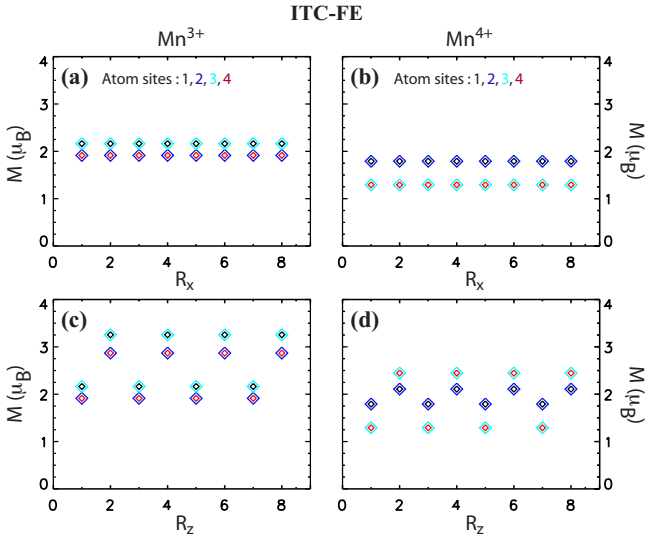

FIG. 3. (Color online) For the ITC-FE phase, the magnitude of the magnetic moment, *M*, of the Mn^{3+} and that of the Mn^{4+} ion shown in Fig. 2 are plotted over different chemical unit cells [(a) and (b)] along the *a* axis and [(c) and (d)] along the *c* axis.

the ITC-FE phase can be approximately produced by our Landau theory with only one order parameter.

Our magnetic structure shown in Fig. 2 is almost the same as the previously reported structure that was obtained by Kimura *et al.*[45] without assuming any particular symmetry: the *ab* components of Mn^{4+} moments are collinear along the *c* axis [Fig. 2(a)]; the *ac* components [Fig. 2(b)] and *bc* components [Fig. 2(c)] of Mn^{4+} moments form cycloidal spirals along the *c* axis. The zigzag chain formed by Mn^{4+} and Mn^{3+} on the *ab* plane is also nearly collinear [Fig. 2(d)]. The magnitudes of the Mn^{3+} and Mn^{4+} moments do not change along the *a* axis over different chemical unit cells while they oscillate between two values along the *c* axis (see Fig. 3). According to the spin-current mechanism, the *ac* and *bc* spirals can give rise to electric polarization, **P**, along *a* and *b* axes, respectively. **P** induced by the *ac* spirals of neighboring chains are, however, in opposite directions and, thus, cancel with each other [Fig. 2(b)], while **P** induced by the *bc* spirals are in the same *b* direction [Fig. 2(c)], resulting in the bulk electric polarization along the *b* direction as observed experimentally. On the other hand, the magnetostriction model[34] can be applied to the chain of Mn^{4+}-Mn^{3+}-Mn^{3+}-Mn^{4+} ions along the *b* axis that are more or less parallel and are arranged in a sequence of ↑↑↓↑. This spin configuration will give *a* and *b* displacements of frustrated Mn^{3+} ions. But *a*-direction displacement is canceled out with neighboring spin configuration so that it leads to a strong **P** along the *b* axis.[19] This conclusion agrees with that of Landau theory.

For the LTI-FE phase we fit to a structure without assuming any symmetry constraints. The symmetry constraints we have invoked to fit the ITC-FE phase are specific to continuous transitions and, thus, may apply to phases which can be reached by one or more continuous transitions, as is the case for the ITC-FE phase (this is discussed in Refs. 48 and 6). Since there is apparently no path to reach the LTI-FE phase from the paramagnetic phase via only continuous transitions, we fit the data for this phase to a structure without assuming any symmetry constraints. The best fit was obtained with the optimal parameters that are listed in Table IV and the resulting magnetic structure is illustrated in Fig. 4. For the LTI-FE phase, the only magnetic structure reported so far is the one that was obtained by a neutron powder-diffraction study.[19] In that magnetic structure, in each Mn^{4+} chain along the *c* axis the moments are nearly collinear with a sinusoidally modulated amplitude. In the *ab* plane, Mn^{4+} and Mn^{3+} moments are nearly collinear and coplanar, and along the Mn^{4+}-Mn^{3+} zigzag chains, their magnitudes follow a sinusoidal modulation yielding almost zero moments for certain positions. Our incommensurate magnetic structure, however, is different. The magnitudes of Mn^{4+} and Mn^{3+} moments weakly fluctuate [see Figs. 5(a)–5(d)] along the *a* and the *c* axis. The more prominent feature is that they form complex spiral structures along the *a* and *c* axes. First, the *ab* components of the Mn^{4+} moments rotate about the *c* axis [see Fig. 4(a)], forming a longitudinal spiral. Second, the *ac* and *bc* components of the Mn^{4+} form cycloidal spirals along the *c* axis [Figs. 4(b) and 4(c)] as in the ITC-FE phase. Third, the *ab* components of all Mn ion moments form a cycloidal spiral along the *a* axis [see Fig. 4(d)]. By the spin-current mechanism, a longitudinal spiral does not give rise to any electric polarization. When we add all **P**'s induced by the three cycloidal spirals [(b)–(d)], the magnitude of the bulk **P** along *b* axis is much weaker than that of the ITC-FE phase, as experimentally observed. Application of the magnetostriction mechanism ($\mathbf{P} \propto \mathbf{S}_i \cdot \mathbf{S}_j$) on our LTI-FE spin structure also leads to a weak **P** along *b* axis because the Mn^{4+}-Mn^{3+} moments along the *b* axis [inside red and blue ellipses in (d)] are now almost

TABLE IV. Magnetic parameters for the magnetic structure of the LTI-FE phase [$\mathbf{k_{IC}}=(1/2+\delta_a,0,1/4+\delta_c)$ with $\delta_a=-0.02$ and $\delta_c=0.038$] of YMn_2O_5, obtained by fitting FCD and PND data at 10 K. Listed are the parameters for the moments in a chemical unit cell. Each component of their magnetic moments is given by $M_i=A_i\cos(\phi_i)$. The magnetic moments of the corresponding ions in a chemical unit cell separated by a distance **R** from the original unit cell can be estimated by $M_i=A_i\cos(\mathbf{k_{IC}}\cdot\mathbf{R}+\phi_i)$. Errors for all parameters are given within parenthesis. The optimal χ^2 and the R factor were obtained to be 8.3 and 7.70%, respectively, where the number of data points, N, is 269 and the number of parameters including an overall scale factor N_p is 49.

	Site	A_a (μ_B)	ϕ_a (rad)	A_b (μ_B)	ϕ_b (rad)	A_c (μ_B)	ϕ_c (rad)
Mn^{3+}	1	2.37(6)	0.99(6)	1.84(6)	−0.41(5)	0.26(5)	1.16(24)
	2	1.57(9)	1.06(7)	1.52(6)	−0.26(6)	1.04(6)	1.34(8)
	3	−2.79(7)	−0.16(6)	−1.36(6)	−1.65(7)	0.84(6)	−1.32(10)
	4	2.61(8)	−0.13(6)	1.17(7)	−1.91(8)	0.73(6)	0.75(9)
Mn^{4+}	1	−1.32(9)	0.87(6)	−1.59(6)	−0.74(4)	−0.66(7)	0.96(10)
	2	1.91(7)	−0.49(5)	1.05(6)	−2.30(7)	0.61(6)	0.88(12)
	3	1.69(7)	0.17(5)	0.98(5)	−1.45(8)	−0.89(6)	−1.63(9)
	4	−1.26(8)	1.51(5)	−1.45(6)	0.01(4)	−0.50(7)	−4.11(12)

orthogonal. By the way, we have found that the bulk **P** induced by the spin-current mechanism would have a nonvanishing a component, as well as a b component of the resulting total **P** of the LTI-FE phase. Thus our results also predict that in the ITC-FE phase the spontaneous electric polarization will have a nonzero component along **a**, although it may be quite small.

IV. DISCUSSION

Our finding that YMn_2O_5 has complex spiral structures in both ITC-FE and LTI-FE phases has important theoretical implications in the field of multiferroics. First, the spiral structures of YMn_2O_5 are consistent with both the spin-current model and the magnetostriction model to explain magnetoelectric coupling. Second, according to the spin-current mechanism the incommensurate structure of YMn_2O_5 may induce weak **P** along the a axis as well as along the b axis. This will have to be checked by measuring **P** as a function of temperature with an application of an external electric field along the a axis. According to a symmetry-based Ginzburg-Landau theory[40] when the higher order terms of the magnetic order parameters and umklapp magnetoelectric interactions are considered in the phase with $\mathbf{k_{IC}}=(1/2+\delta_a,0,1/4+\delta_c)$ which has nonzero δ_a, the weak spontaneous polarization **P** should appear in all directions. Indeed, electric polarization has recently been observed along the a axis in an incommensurate phase of $TmMn_2O_5$.[49] This might be consistent with our finding that an incommensurate spin structure of AMn_2O_5 can induce **P** along the a

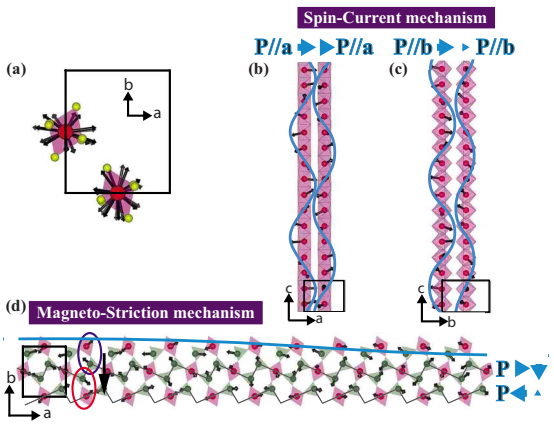

FIG. 4. (Color online) Magnetic structure of the LTI-FE phase of YMn_2O_5 that is projected onto different planes: (a) ab plane, (b) ac plane, (c) bc plane, and (d) ab plane. In (d) thin gray lines represent the Mn^{4+}-Mn^{3+}-Mn^{4+} zigzag chains. The symbols and colors were used in the same way as in Fig. 2.

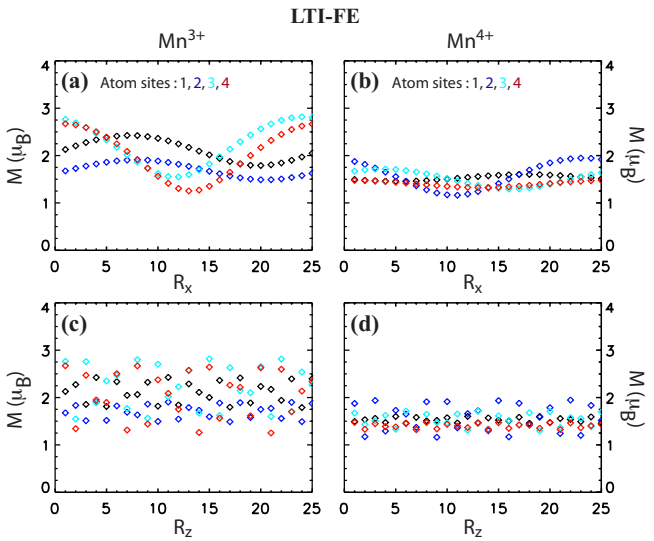

FIG. 5. (Color online) For the LTI-FE phase, the magnitude of the magnetic moment, M, of the Mn^{3+} and that of the Mn^{4+} ion shown in Fig. 4 are plotted over different chemical unit cells [(a) and (b)] along the a axis and [(c) and (d)] along the c axis.

axis. Of course, we need to keep in mind that only two types of chains in this compound were considered for the spin currents: the Mn^{4+} chains along the *c* axis and the Mn^{4+}-Mn^{3+} zigzag chains in the *ab* plane. Also the coefficient α was assumed to be the same for the two different types of chains. It should also be noted that the spin-current model is a simple theory for the magnetoelectric effect of two neighboring magnetic moments. The application to a real material would require some complicated modifications to the theory. Nonetheless, our simple analysis explains why **P** weakens considerably at the ITC-FE to the LTI-FE phase transition as observed experimentally. It is also possible that both the mechanisms might be in play in this complex system. The complex magnetic structures of YMn_2O_5 reported here will impose a strict restriction on the theoretical endeavor.

ACKNOWLEDGMENTS

We thank L. C. Chapon and P. G. Radaelli for helpful discussions. Work at University of Virginia was supported by the U.S. DOE through Grant No. DE-FG02-07ER46384, work at Rutgers by the NSF under Grant No. NSF-DMR-0520471, and work at JAEA by Japan Grant-in-Aid for Scientific Research on Priority Areas under Grant No. 19052004/19052008. M.K. was supported by the Swiss NSF.

*shlee@virginia.edu

[1] T. Kimura, T. Goto, H. Shintani, K. Ishizaka, T. Arima, and Y. Tokura, Nature (London) **426**, 55 (2003).
[2] N. Hur, S. Park, P. A. Sharma, J. S. Ahn, S. Guha, and S.-W. Cheong, Nature (London) **429**, 392 (2004).
[3] N. A. Hill, J. Phys. Chem. B **104**, 6694 (2000).
[4] N. A. Spaldin and M. Fiebig, Science **309**, 391 (2005).
[5] M. Fiebig, J. Phys. D: App. Phys. **38**, R123 (2005).
[6] A. B. Harris, A. Aharony, and O. Entin-Wohlman, J. Phys.: Condens. Matter **20**, 434202 (2008).
[7] A. Kobayashi, T. Osawa, H. Kimura, Y. Noda, N. Kasahara, S. Mitsuda, and K. Kohn, J. Phys. Soc. Jpn. **73**, 3439 (2004).
[8] L. C. Chapon, G. R. Blake, M. J. Gutmann, S. Park, N. Hur, P. G. Radaelli, and S.-W. Cheong, Phys. Rev. Lett. **93**, 177402 (2004).
[9] Y. Koyata and K. Kohn, Ferroelectrics **204**, 115 (1997).
[10] D. Higashiyama, S. Miyasaka, and Y. Tokura, Phys. Rev. B **72**, 064421 (2005).
[11] H. Kimura, Y. Kamada, Y. Noda, K. Kaneko, N. Metoki, and K. Kohn, J. Phys. Soc. Jpn. **75**, 113701 (2006).
[12] N. Hur, S. Park, P. A. Sharma, S. Guha, and S.-W. Cheong, Phys. Rev. Lett. **93**, 107207 (2004).
[13] D. Higashiyama, S. Miyasaka, N. Kida, T. Arima, and Y. Tokura, Phys. Rev. B **70**, 174405 (2004).
[14] W. Ratcliff II, V. Kiryukhin, M. Kenzelmann, S.-H. Lee, R. Erwin, J. Schefer, N. Hur, S. Park, and S.-W. Cheong, Phys. Rev. B **72**, 060407(R) (2005).
[15] R. A. Ewings, A. T. Boothroyd, D. F. McMorrow, D. Mannix, H. C. Walker, and B. M. R. Wanklyn, Phys. Rev. B **77**, 104415 (2008).
[16] S. Kobayashi, T. Osawa, H. Kimura, Y. Noda, I. Kagomiya, and K. Kohn, J. Phys. Soc. Jpn. **73**, 1031 (2004).
[17] M. Fukunaga, K. Nishihata, H. Kimura, Y. Noda, and K. Kohn, J. Phys. Soc. Jpn. **76**, 074710 (2007).
[18] S. Kobayashi, T. Osawa, H. Kimura, Y. Noda, I. Kagomiya, and K. Kohn, J. Phys. Soc. Jpn. **73**, 1593 (2004).
[19] L. C. Chapon, P. G. Radaelli, G. R. Blake, S. Park, and S.-W. Cheong, Phys. Rev. Lett. **96**, 097601 (2006).
[20] S. Kobayashi, H. Kimura, Y. Noda, and K. Kohn, J. Phys. Soc. Jpn. **74**, 468 (2005).
[21] A. Inomata and K. Kohn, J. Phys.: Condens. Matter **8**, 2673 (1996).
[22] M. Uga, N. Iwata, and K. Kohn, Ferroelectrics **219**, 55 (1998).
[23] C. R. dela Cruz, B. Lorenz, Y. Y. Sun, Y. Wang, S. Park, S.-W. Cheong, M. M. Gospodinov, and C.W. Chu, Phys. Rev. B **76**, 174106 (2007).
[24] R. P. Chaudhury, C. R. dela Cruz, B. Lorenz, Y. Sun, C.-W. Chu, S. Park, and Sang-W. Cheong, Phys. Rev. B **77**, 220104(R) (2008).
[25] C. R. dela Cruz, B. Lorenz, Y. Y. Sun, C. W. Chu, S. Park, and S.-W. Cheong, Phys. Rev. B **74**, 180402(R) (2006).
[26] C. R. dela Cruz, F. Yen, B. Lorenz, M. M. Gospodinov, C. W. Chu, W. Ratcliff, J. W. Lynn, S. Park, and S.-W. Cheong, Phys. Rev. B **73**, 100406(R) (2006).
[27] A. Ikeda and K. Kohn, Ferroelectrics **169**, 75 (1995).
[28] H. Katsura, N. Nagaosa, and A. V. Balatsky, Phys. Rev. Lett. **95**, 057205 (2005).
[29] M. Kenzelmann and A. B. Harris, Phys. Rev. Lett. **100**, 089701 (2008).
[30] M. Kenzelmann, G. Lawes, A. B. Harris, G. Gasparovic, C. Broholm, A. P. Ramirez, G. A. Jorge, M. Jaime, S. Park, Q. Huang, A. Ya. Shapiro, and L. A. Demianets, Phys. Rev. Lett. **98**, 267205 (2007).
[31] T. A. Kaplan and S. D. Mahanti, arXiv:0808.0336 (unpublished).
[32] I. A. Sergienko and E. Dagotto, Phys. Rev. B **73**, 094434 (2006).
[33] A. B. Harris, T. Yildirim, A. Aharony, and O. Entin-Wohlman, Phys. Rev. B **73**, 184433 (2006).
[34] S.-W. Cheong and M. Mostovoy, Nature Mater. **6**, 13 (2007).
[35] M. Kenzelmann, A. B. Harris, S. Jonas, C. Broholm, J. Schefer, S. B. Kim, C. L. Zhang, S.-W. Cheong, O. P. Vajk, and J. W. Lynn, Phys. Rev. Lett. **95**, 087206 (2005).
[36] T. Arima, A. Tokunaga, T. Goto, H. Kimura, Y. Noda, and Y. Tokura, Phys. Rev. Lett. **96**, 097202 (2006).
[37] Y. Yamasaki, S. Miyasaka, Y. Kaneko, J.-P. He, T. Arima, and Y. Tokura, Phys. Rev. Lett. **96**, 207204 (2006).
[38] G. Lawes, A. B. Harris, T. Kimura, N. Rogado, R. J. Cava, A. Aharony, O. Entin-Wohlman, T. Yildirim, M. Kenzelmann, C. Broholm, and A. P. Ramirez, Phys. Rev. Lett. **95**, 087205 (2005).
[39] A. B. Harris, Phys. Rev. B **76**, 054447 (2007); **77**, 019901(E) (2008).
[40] A. B. Harris, M. Kenzelmann, A. Aharony, and O. Entin-Wohlman, Phys. Rev. B **78**, 014407 (2008).
[41] M. Mostovoy, Phys. Rev. Lett. **96**, 067601 (2006).

[42] J. J. Betouras, G. Giovannetti, and J. van den Brink, Phys. Rev. Lett. **98**, 257602 (2007).
[43] J. A. Alonso, M. T. Casais, M. J. Martínez-Lope, J. L. Martínez, and M. T. Fernández-Díaz, J. Phys.: Condens. Matter **9**, 8515 (1997).
[44] C. Vecchini, L. C. Chapon, P. J. Brown, T. Chatterji, S. Park, S.-W. Cheong, and P. G. Radaelli, Phys. Rev. B **77**, 134434 (2008).
[45] H. Kimura, S. Kobayashi, Y. Fukuda, T. Osawa, Y. Kamada, Y. Noda, I. Kagomiya, and K. Kohn, J. Phys. Soc. Jpn. **76**, 074706 (2007).
[46] F. Tasset, J. Magn. Magn. Mater. **129**, 47 (1994).
[47] G. R. Blake, L. C. Chapon, P. G. Radaelli, S. Park, N. Hur, S.-W. Cheong, and J. Rodríguez-Carvajal, Phys. Rev. B **71**, 214402 (2005).
[48] A. B. Harris, A. Aharony, and O. Entin-Wohlman, Phys. Rev. Lett. **100**, 217202 (2008).
[49] Y. Noda *et al.* (unpublished).